Design, Implementation and Operation of a Sparse Aperture Imaging Satellite Testbed

Soon-Jo Chung*
617-253-6685, sjchung@mit.edu

David W. Miller†
617-253-3288, millerd@mit.edu

Space Systems Laboratory, Department of Aeronautics and Astronautics, MIT
Cambridge, Massachusetts 02139, USA

Abstract . In order to better understand the technological difficulties involved in designing and building a sparse aperture array, the challenge of building a white light Golay-3 telescope was undertaken. The MIT Adaptive Reconnaissance Golay-3 Optical Satellite (ARGOS) project exploits wide-angle Fizeau interferometer technology with an emphasis on modularity in the optics and spacecraft subsystems. Unique design procedures encompassing the nature of coherent wavefront sensing, control and combining as well as various system engineering aspects to achieve cost effectiveness, are developed. To demonstrate a complete spacecraft in a 1-g environment, the ARGOS system is mounted on a frictionless air-bearing, and has the ability to track fast orbiting satellites like the ISS or the planets. Wavefront sensing techniques are explored to mitigate initial misalignment and to feed back real-time aberrations into the optical control loop. This paper presents the results and the lessons learned from the conceive, design, implement and operate phases of ARGOS. A preliminary assessment shows that the beam combining problem is the most challenging aspect of sparse optical arrays. The need for optical control is paramount due to tight beam combining tolerances. The wavefront sensing/control requirements appear to be a major technology and cost driver.

Keywords: sparse aperture, multiple-aperture optical systems, telescopes, fizeau interferometer, phased telescope array**.**

1 Introduction

The quest for finer angular resolution in astronomy will inevitably lead to larger apertures. Unfortunately, the primary mirror diameter for space telescopes is limited by volume and mass constraints of current launch vehicles as well as the scaling laws of manufacturing costs[1]. Since the cost of monolithic optics increases faster than diameter squared, and mirrors such as the Hubble Space Telescope's are already at the edge of what is financially feasible, efforts are ongoing to break this trend by employing exotic technologies such as deployed segmented mirror telescope, and sparse aperture optics using interferometry.

Similiar to the ground-based Multiple Mirror Telescope (MMT), space based imaging can be accomplished with a segmented monolithic mirror. NASA's Next Generation Space Telescope (NGST) features a 6-meter monolithic mirror with deployable lightweight filled apertures. Another breakthrough technology is to explore space interferometry. Numerous NASA future telescope missions such as the Space Interferometry Mission (SIM) and the Terrestrial Planet Finder (TPF) are based on Michelson interferometer technology. Basically, Interferometers deploy more than two apertures and combine multiple beams to achieve higher angular resolution, astrometry and nulling depending on the mission requirements.

Whereas Michelson interferometers feed lights from independent collectors to a beam combiner to obtain interfered fringes over a period of time, Fizeau interferometers produce direct image with full instant u-v coverage. Hence, the Fizeau is suitable for optical imaging of extended objects and rapidly changing targets. In contrast to the long baselines of Michelson interferometers, Fizeau interferometry systems tend to have compact telescope arrays.

* Graduate Research Assistant, Space Systems Laboratory
† Associate Professor, Department of Aeronautics and Astronautics

Two types of optical Fizeau interferometers are shown in Figure 1. The common secondary array type shares one common secondary mirror, thus giving little or zero central obstruction. The second type, phased telescope array (sparse array) is chosen for ARGOS over the common secondary because it allows the system to utilize off-the-shelf telescopes providing more opportunity to explore modularity than the common secondary array. More complicated relay optics and beam combing are however expected.

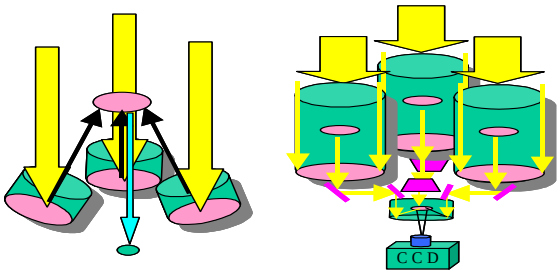

FIG. 1: Two types of Fizeau interferometers: The common secondary mirror array (left) and the phased telescope array (right)

An optimal imaging configuration designed for sparse arrays was first proposed by Golay[2]. Sparse arrays are promising for applications that do not require extremely high sensitivity (bright source present) and allow for a rather limited field-of-view (FOV)[4,6].

1.1 Overview of ARGOS

In order to better understand the technological difficulties involved in designing and building a sparse aperture array, the challenge of building a white light Golay-3 telescope was undertaken. The MIT Adaptive Reconnaissance Golay-3 Optical Satellite (ARGOS)[5] project exploits wide-angle Fizeau interferometer technology with an emphasis on modularity in the optics and spacecraft subsystems.

The objective of the Adaptive Reconnaissance Golay-3 Optical Satellite (ARGOS) project is to demonstrate the practicality of a modular architecture for space-based optical systems.In order to understand what is expected from ARGOS, we have broken down our objective into its key components.

First, the word demonstrate implies that ARGOS will operate in a mode representative of a real-world application. The telescope must be able to capture an image of a real target, such as the International Space Station (ISS) or a celestial body. Furthermore, the satellite must be capable of remote operation; it shoud receive commands from a ground station that is not physically connected to the satellite.

Practicality implies that our design competes with the quality to cost ratio of current technology. ARGOS's angular resolution as a function of cost must be comparable to current systems. The design must also have an ease of manufacturability comparable to current systems.

Modular refers to both the satellite architecture and the optics. Modular architecture implies assembling the system out of modules (identical, similar or dissimilar) that facilitate fabrication, integration, and testing. The design should maximize simplicity of interfaces and strive for standardization of components. To achieve this standardization and to hold down manufacturing costs, ARGOS will maximize usage of commercial off-the-shelf (COTS) items. Modular optics generate image data from similar sub-apertures as opposed to a single monolithic system. Active optics control must then be able to coherently combine the light from the separate apertures.

Space-based implies that the ARGOS system must exhibit the functionality of a satellite. It must be able to track a slewing object. Moreover, the satellite must be self-contained, which entails power restrictions, communications, contamination protection, and time critical data transfer.

Figure 2 highlights the key functional and operational

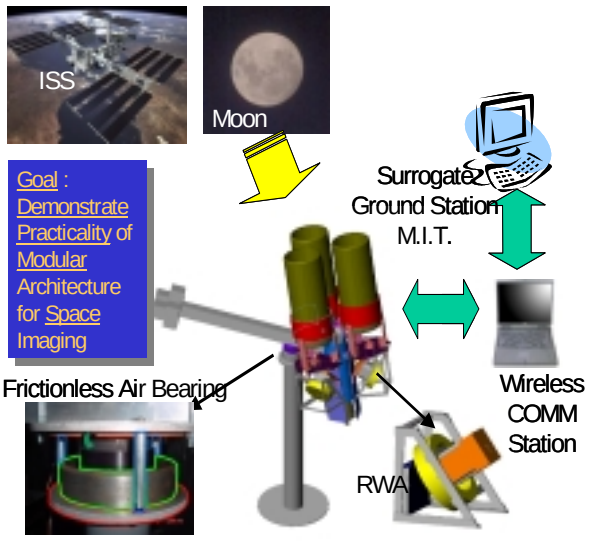

FIG. 2: Overview of ARGOS system

objectives. To demonstrate a complete spacecraft in a 1-

g environment, the ARGOS system is mounted on a frictionless air-bearing, and has the ability to track fast orbiting satellites like the International Space Station (ISS) as well as point stars. Modular architecture design emphasizes the use of replicated components and quick connections. The system consists of three identical apertures arranged in a Golay-3 distribution. The light from these telescopes is combined in a center module and transmitted to a Charge-Coupled Device (CCD). W wavefront sensing techniques are explored to mitigate initial misalignment and to feed back real-time aberrations into the optical control loop. The end result is an image as good as the image received from a monolithic telescope using a single aperture. ARGOS operates autonomously and in a self-contained manner while a wireless ground station downloads images and telemetry information. The primary functional and operational requirements of ARGOS are prescribed in Table 1.

TABLE 1: Key functional and operational requirements

Key Requirements	
Angular Resolution	0.35 arcsec at visible
Operating Wavelength	400-700 nm (Visible)
Field of View (FOV)	3 arcmin * 3 arcmin
Field of Regard (FOR)	120 °
Signal to Noise Ratio (SNR)	100
ACS Pointing Accuracy	+/- 1 arcmin
Image Acquisition Time	20 images/ hour (max)
Autonomous Operation Time	up to 1 continuous hour

1.2 Previous Work and Comparisons

There are many past and ongoing long baseline ground-based Michelson interferometer projects including the Keck interferometer and Palomar Testbed Interferometer (PTI). In addition, NASA is planning to launch innovative space-based interferometers, e.g. SIM, TPF. However, successful sparse aperture telescope projects using Fizeau beam combining are rare.

A notable project in the area of phased telescope array is the Multipurpose Multiple Telescope Testbed (MMTT)[7] by Air Force Research Laboratory (AFRL). The MMTT consists of four 20-cm-aperture telescopes phased together with a 15-arcmin field-of-view (FOV). As opposed to ARGOS which operates in a real environment tracking celestial objects, the MMTT is built for laboratory use only using laser point sources. The MMTT is the first wide FOV phased array telescope measuring combined point spread function (PSF). The Air Force is also developing the UltraLITE[3] earth imaging satellite using Golay-6 array Fizeau interferometry.

To achieve coherent phased beam combining, the images should be superimposed on CCD with an accuracy of a fraction of the operating wavelengths. We can infer that high precision wavefront error (WFE) sensing is critical to accomplish this goal. The MMTT employs a traditional laser interferometer metrology to sense WFE. The cost of the complicated optics in the MMT sensor system is prohibitively high, and it occupies a lot of space for this series of optics, which is not feasible for compact space-borne observatories. The Multi Aperture Imaging Array[8] built by Lockheed Martin demonstrated phase diversity computation techniques for WFE sensing. This sparse array consists of afocal telescopes arranged in a Y-formation that are combined to a common focus in a Fizeau interferometer configuration. It demonstrated the first results of a board band multiple telescope imaging array phased over a significant field of view using the extended image projector in the lab.

The Large Binocular Telescope (LBT)[9] is being built by the University of Arizona and several international institutions. The LBT telescope will have two 8.4 meter diameter primary mirrors phased on a common mounting with a 22.8 meter baseline. Both apertures will be mounted on the same structure, resulting in a system more compact than other current ground-based interferometers.

The ARGOS testbed is the first in-flight sparse aperture array simulating an imaging space-borne observatory in a 1-g environment. Most of the previous sparse aperture array systems do not represent the real world problems such as the vibrational coupling between a spacecraft structure and the wavefront errors propagating through the whole system. If ARGOS succeeds in coherent beam combining, it will be the first sparse aperture array to obtain a phased image of a real target in the sky.

2 Optics Design

2.1 SOCS Framework

Figure 3 shows the Sparse-aperture Optics/Control (SOCS) design framework. The motivations of this SOCS framework are the following.

There have been many interferometric array projects around the world. However, there have been few projects that emphasize cost effective designs with a system engineering approach. Both cost and risk are critical factors particularly for space-based imaging systems. Lack of a system engineering mind in the era of high technological advances in astromical interferometry, adaptive optics and sparse aperture array, caused confusions in identifying key elements and their mutual

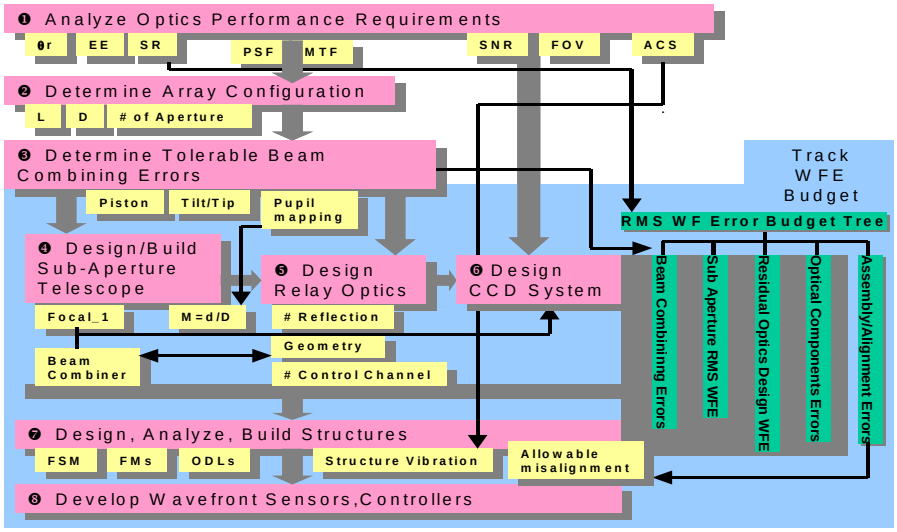

FIG. 3: Sparse-aperture Optics/Control System (SOCS) design flow-down procedures

relations to avoid high-cost systems. In addition, the control engineer and the optics designers must communicate with each other from the early stage of design through the actual implementation to achieve coherent beam combining with interferometric array.

The objective of SOCS is in each design step, to facilitate identification and correlation procedures of design parameters in order to get an optimum cost-effective performance design.

What is unique about this framework is that it explores the benefits of modular architecture in space-borne imaging systems. In other words, we practice design philosophy of cost-effectiveness and manufacturability throughout the design and implementation procedures so as to better understand the impact of the system engineering methodologies on development of space interferometric arrays. Each design step in Figure 3 is briefly described in the following.

(Step 1) Analyze optics performance requirements - define and interpret customer requirements such as angular resolution, strehl ratio (SR) and encircled energy (EE).

(Step 2) Determine an array configuration.- determine a subaperture diameter (D) and the array radius (L) by looking at the point spread functions (PSF) and modulation transfer functions (MTF).

(Step 3) Analyze tolerable beam combing errors and start keeping track of wavefront error budget tree. Using the array configuration from step 2, determine the beam combining tolerances. This analysis is fundamental in understanding the nature of interferometric arrays. Also, construct and update the wavefront error budget trees.

(Step 4) Design a subaperture with an optical precision that meets the WF (wavefront) error budget tree specifications.

(Step 5) Design and build relay optics- determine how many optical reflections will be incorporated into the relay optics. The geometry and the shape of optics controllers are defined. In addition, explore the various methods of beam combining.

(Step 6) Design CCD systems. The relationships between spare aperture array and Signal to Noise Ratio (SNR) are discussed by Roddier[10] and Fienup[11].

(Step 7) Design/ Analyze/ Build Structures. According to the remaining the WF error budgets, calculate the maximum allowable misalignment for each structure (sub-aperture, FSM and ODL actuators, and beam combiner). Also, design the structures to meet the optics requirements (precision stages, precision mounts). Perform Finite Element Model (FEM) analysis.

(Step 8) Implement the wavefront sensors and controllers. - Develop the wavefront sensors and control logics to achieve coherent beam combining.

The detailed design procedures are described in the following sections.

2.2 Determination of Array Configuration

Traditional image quality criteria such as resolution and encircled energy (EE) are inadequate for many sparse aperture or interferometric array applications[12]. Given the angular resolution and encircled energy specifications from the optics requirements, the designers should use the optical performance evaluation tools such as

point spread functions (PSF) and modulation transfer functions (MTF).

A PSF is an irradiance distribution representing the image of an ideal point source. Namely, a PSF is a diffraction limited intensity distribution in response to a point source such as a very distant star. We can derive the Strehl ratio, encircled energy and angular resolution from the PSF. The Strehl ratio is the ratio between the on-axis intensity of an aberrated beam and the on-axis intensity of an unaberrated beam. Encircled energy is defined as the intensity energy enclosed under the PSF envelope as a function of off-axis angle. Our purpose of using encircled energy is to measure the relative size between mainlobe and sidelobes.

When we look at an extended objects such as the Moon and a faint distant nebula, evaluation of an optical system is far more complex than by simply looking at a point source response (PSF). MTF is a better metric to evaluate the contrast (modulation) transfer characteristic of an extended object. In Figure 4, the PSF and MTF plots of D=0.21m (ARGOS subaperture diameter) and L=0.12m (blue), 0.19m (red), 0.3m (black) are shown. A perfect monolithic array, free of optical aberrations, has a linearly decreasing MTF contrast characteristic (See the blue MTF line of Figure 4). In case of a sparse array, the MTF suffers a contrast loss in the mid spatial frequency range as shown in Figure 4. We can see the MTF plot with L=0.3m exhibits two zero values rather than one. The first zero denoted by Fr is the practical spatial cut-off frequency, and defines the "practical resolution limit". The Fc is the cut-off frequency, whose inverse indicates an angular resolution under the normal condition that there is no Fr (another zero region) before Fc. So the larger Fc or Fr is, the better angular resolution a sparse array will achive.

As opposed to a monolithic aperture, the method of Full-Width-Half-Maximum (FWHM) or reading the first minima of a PSF plot is not sufficient to determine the angular resolution. Assuming that angular resolution is fully determined by the array size, PSF can reveal the highest achievable angular resolution. This assumption holds especially for very large baseline Michelson interferometers. We can observe in Figure 4, that the mainlobe size of the PSF plot is getting smaller, indicating improving angular resolution as we increase the array size L. The Fizeau interferometer, however, requires an instant full u-v coverage, which limits our practical resolution. In addition, as discussed above, the contrast loss of mid-spatial frequency range should be avoided. So if the practical cut-off frequency(Fr) is less than the normal cut-off frequency(Fc), Fr determines the limiting

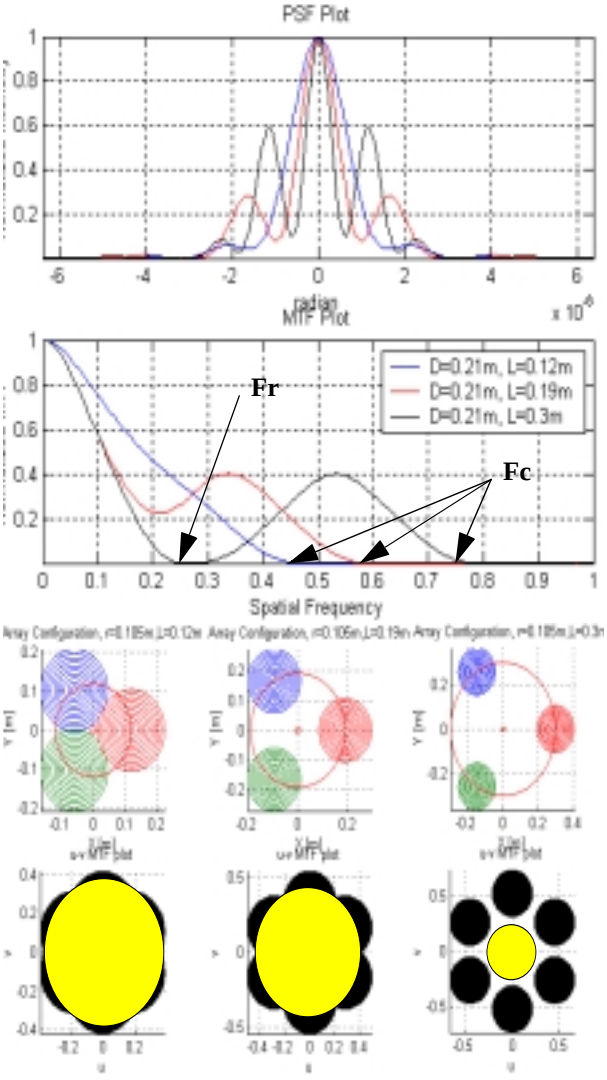

FIG. 4: PSF and MTF plots when D=0.21m and L = 0.12m (blue), 0.19m (red), 0.3m (black). The corresponding array configurations are shown below the PSF-MTF plot. The black-yellow figure is a MTF plot. Yellow circles indicate the practical cut-off frequency.

angular resolution. In other words, there should be no zero region before the MTF reaches Fc.

As we increase L, the array becomes more sparse, which, as a result, boosts the heights of sidelobes on the PSF plots. The MTF plot of L=0.3m (black in Figure 4) has two zeros while others have only one. It means the resolution is limited not by Fc but Fr, whose inverse is an angular resolution of one single aperture (1.22 * wavelength/D). So the sparse array has no advantage over one subtelescope. As L decreases further from L=0.3m, the Fr becomes equal to Fc and no more singu-

lar point exists between zero spatial frequency and Fc as we can see in the uv-MTF plots of Figure 4.

When L=0.12m, in which three apertures touch each other, the MTF plot almost resembles that of one monolithic aperture, which is very desirable. But such an array results in no more than a Multiple Mirror Telescope(MMT) sacrificing the possibility of achieving a better angular resolution. The array configuration of the ARGOS is selected to L = 0.19185 m for D=0.21 m (8 inch) subtelescopes, and it gives a better theoretical angular resolution of 0.35 arcsec rather than 0.55 arcsec of a single aperture, as well as a reasonable MTF characteristic.

2.3 Beam Combining Errors

There are three major wavefront errors that need to be controlled at the beam combiner's focus in order to achieve phased beam combining. Those errors are Optical Path Difference (OPD) - piston error, Tilt/Tip error, and lateral pupil mapping error.

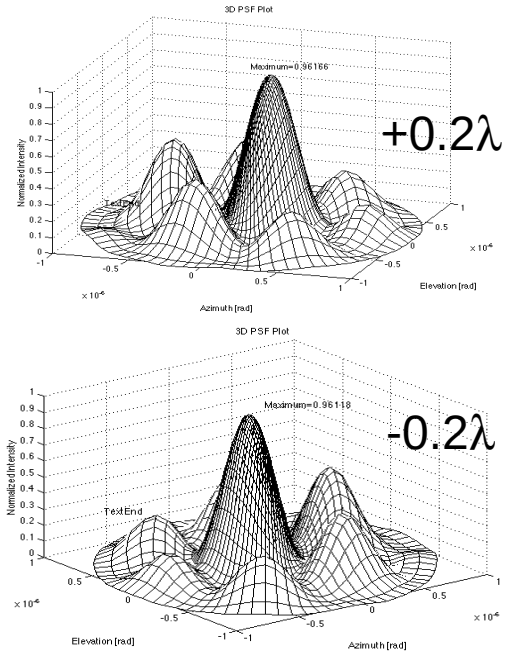

FIG. 5: 3D PSF plot of Golay-3 array with a piston error of +/- 0.2 waves with respect to other apertures

2.3.1 OPD (Piston) Error

We can plot the effects of OPD errors using the interferometry equation given by Mennesson[13].

$$I \propto \left|\frac{\pi D(1+\cos(r))}{\lambda}\right|^2 \left|\frac{J_1(\pi D \sin r/\lambda)}{\pi D \sin r/\lambda}\right|^2 \left|\sum_{k=1}^{n} e^{j2\pi(L_k r/\lambda)\cos(\delta_k-\theta)} e^{j\phi_k}\right|^2$$

Figure 5 shows how the PSF changes when we add OPD error into one of three apertures. As the piston error increases, two major deviations develop over the envelope of the PSF. First, the main envelope shifts in the direction of the piston error. The resultant direction of the envelope shift is the vector sum of phase (piston) error directions weighted by the amount of error. Secondly, the peak intensity gets reduced compared to the normal PSF without any piston errors resulting in a reduced Strehl Ratio (SR). The size of the mainlobe also expands showing a degraded angular resolution (See Figure 6).

Our piston error tolerance is derived from the observations made above. When a piston error is 0.1λ, the peak intensity is 98% of the normal intensity (SR dropped from 0.848 to 0.833, but still above the diffraction limited SR=0.8). The beam combining piston error tolerance = 0.1λ = 55nm.

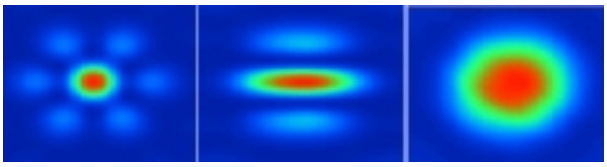

FIG. 6: PSF plot of Golay-3 array with zero OPD, 0.5 λ OPD , and 1.0 λ OPD, from the left to the right.

2.3.2 Tilt/Tip Error

The approach employed here to analyze tilt errors is to further segment each aperture to smaller elements. Then we can imagine 3 aperture golay array consisting of numerous tiny apertures as shown in Figure 7. The point spread function is calculated by summing up all the interference from each element. The phase difference at the central point due to tilt errors are added to the interference term of the Mennesson's equation[13]. We can find the detrimental effects of tilt errors shown in Figure 8. The maximum intensity is reduced to 64% of its original value without any tilt errors. By reading the SR values of the PSF plots under the influence of tilt errors, the maximum allowable tilt error at the beam combining section is determined. This FEM method predicts the tilt tolerance between each beam entering

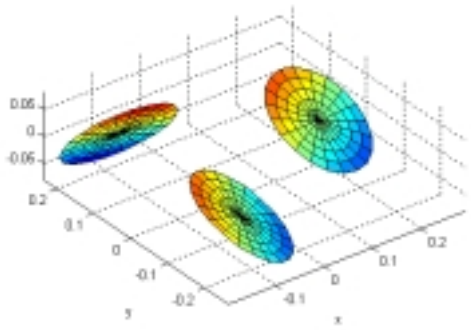

FIG. 7: The geometry set-up of the array under the influence of exaggerated tilt errors

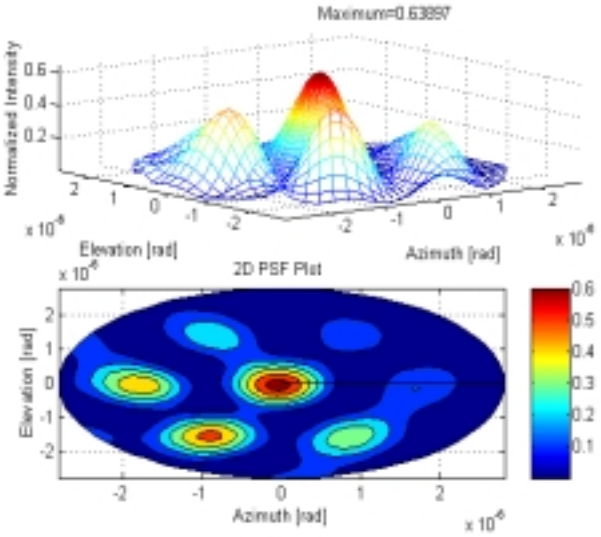

FIG. 8: PSF plot under the following tilt errors: X, Y Tilt of Aperture 1=0, Aperture 2: X tilt=1.0e-4 degree, Ytilt=0, Aperture 3: Xtilt=0,Ytilt= -1.0e-4 degree.

the beam combiner should be less than 20 μ degrees (0.072 arcsec = 0.35 μrad).

2.3.3 Lateral Pupil Mapping Error

If coherent imaging is to be achieved over any significant field-of-view (FOV), the pupil mapping process must be performed such that the exit pupil is an exact (scaled) replica of the entrance pupil[4]. This constraint is commonly called the golden rule of beam combining. Depicted in Figure 9, the golden rule of beam combining can be stated as following.

$$m_a = \frac{D}{d} \quad \text{and} \quad m_t = \frac{B}{b} \quad \text{Golden Rule: } m_a = m_t$$

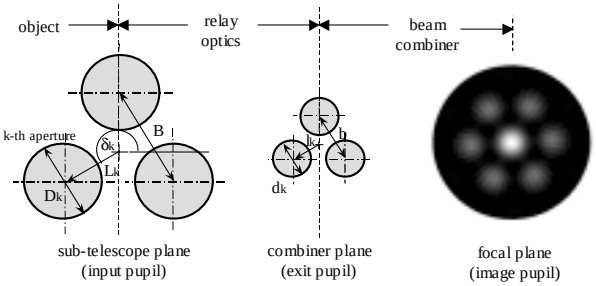

FIG. 9: A golden rule of beam combining, pupil mapping

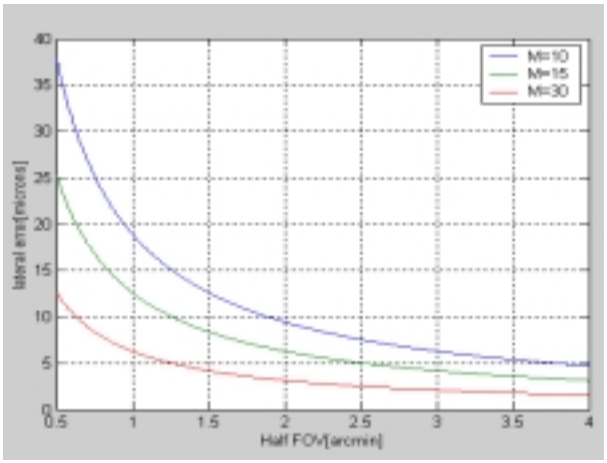

FIG. 10: Tolerable pupil mapping error depending on FOV

D is the diameter of a subaperture while d is the compressed exit beam size of a subaperture. B is the baseline length between apertures while b is the distance between compressed beams when they enter the beam combiner.

Figure 10 shows a graph of tolerable lateral pupil error vs. half FOV angle. Since the magnification (compression) of the ARGOS subaperture is 10 (210 mm to 21mm collimated beam), and our full-angle FOV is around 3 arc min, more than 12 microns is allowable for shear error at the common beam combiner.

2.4 Sub-Aperture

The overall cost of the ARGOS optics system could be significantly reduced by selecting one of the highest precision optics commercially off-the-shelf (COTS) telescope. However, it is necessary to customize a collimating lens to convert a Dall-Kirkham-type focal telescope to an afocal telescope with a compression ratio of 10. The collimating lens is placed into the baffle of the telescope to make the system compact.

The collimating lens went through two rounds of down selecting before deciding what type of lens to use. In the first round, we needed to decide whether to use a cemented doublet, or a regular air space doublet. The air spaced doublet is actually significantly more expensive than the cemented doublet. There are several reasons. The cemented doublet has two exposed surfaces that need to be treated with an anti-reflective coating instead of four in the case of the air spaced doublet. The surfaces between the two glasses in the cemented doublet can be polished to a lesser accuracy than those exposed to air since the index of diffraction does not change much from one glass type to the next and therefore wavefront errors are less destructive. A lens cell needs to be designed for the separate lenses and the lenses need to be mounted to very high tolerances. A cemented doublet does not need a lens cell since the two lenses are bonded. Both types of lenses can be designed to perform almost identically, therefore a cemented doublet is chosen to save the cost.

A second round of down selecting was done on several different doublets that were optimized extensively by ZEMAX (a ray-tracing software by Focus-Software). The difference between these doublets is the material they were made of. One drawback of the cemented doublet is that it has bonded glasses, therefore if there is a change of temperature, the doublet may fail. Although a doublet with CaF2 performs best in reducing chromatic aberrations, the high CTE of CaF2 (18.3) forced us to find other glass combination for efficient achromatic doublet design. Smith[14] suggests FK51 (as a crown element) with a KzFS or LaK glass (as a flint). Although the maximum focal shift range can be reduced to 247 microns with FK51-KzFS11, it is not the best choice due to the residual aberrations (RMS wavefront errors predicted by ZEMAX). The final FK51-BaK2 design achieves 271.6 micron chromatic focal shift range.

2.5 Relay Optics and Beam Combiner

2.5.1 Design of OPD and Tilt/Tip Controller

When strictly looking at two designs of optical delay lines (ODL) in Figure 11, a perpendicular design seems to offer the most benefits. For the perpendicular design, a multi-axis FSM could be used to generate the required tip/tilt actuations as well as fine optical path difference control. FSM's have very fine resolutions so depending on them for fine OPD control will allow us to have a cheaper coarse control for the ODL.

When the parallel ODL design is coupled with a FSM (Figure 11), the resulting design is very simple and more cost-effective than the perpendicular design. This design

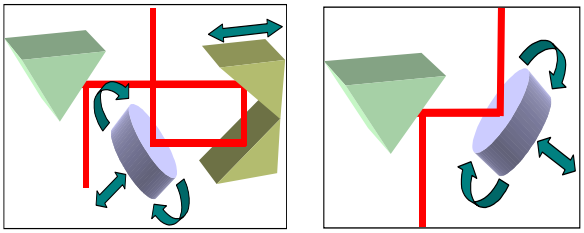

FIG. 11: Perpendicular ODL design with FSM (left) and Parallel ODL design coupled with FSM (right)

cannog perform coarse OPD control but has other characteristics that are better than the perpendicular design. This design is more compact resulting in easier integration with the structural design. In addition, there is no need for a translational stage or rooftop mirror which reduces the cost and control complexity, and there is also a greater total reflectance since there are fewer mirrored surfaces. Fewer mirrored surfaces also lead to fewer structural misalignment errors.

In both the perpendicular ODL design and the parallel ODL design, fine OPD control is coupled with shear control so that ΔFine OPD = ΔShear. The effect that a change in fine OPD would have on shear, is not that great and could be ignored for adjustments < 10 microns. This is because we have much tighter tolerance on piston error (50 nm) than a 12 micron shear error (See Figure 10). A fine resolution multi-axis FSM from Physik Instrumente (PI), capable of controlling the tilt/tip as well as piston motion, was selected for the parallel ODL design.

2.5.2 Pyramidal Mirror and Beam Combiner

The pyramidal mirror turns all three beams 45 deg. into the beam combiner. A custom pyramidal mirror is chosen due to the cost of making one out of regular mirrors. The main reason for the high cost is that we would need to purchase special thin mirrors that cost $1000+, and then mount them to an accuracy of +/- 0.001° (+/- 3.6 arcsec). The pyramid cannot be made from the regular thickness mirrors since they constrain the beam diameter. We customized a pyramidal mirror with a surface accuracy of l/10 peak to valley, +/- 3 arcsec angle error, and 50mm clear aperture. The substrate material is BK7 with a coating of AlSiO (aluminum with silicon monoxide). The reflectance will be approximately 90% in the visible range. The two point spread functions shown in Figure 12 demonstrate how the FSM can compensate for the +/- 3 arcsec errors in the pyramid. In order to compensate for pyramid errors the FSM has to align itself so that the two reflecting surfaces are parallel.

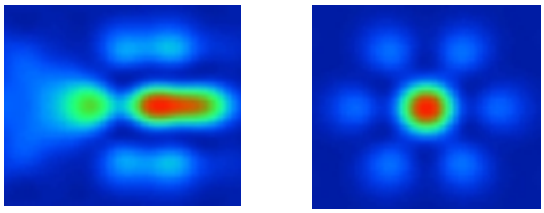

FIG. 12: The PSF of the ARGOS with 3 arcsec tilt error of the pyramidal mirror (SR=0.444, Left). The PSF with FSM correction (SR=0.960, Right)

Two options available for the beam combiner are either reflecting or refracting optics. The reflecting beam combiner is compact when compared to a refractor. Unfortunately, the secondary mirror of a Cassegrain telescope would partially block the three incoming beams in any possible configurations in order to obey the golden rule discussed in the section 2.3.3. A single parabolic mirror was considered, however there was not enough space between the pyramidal mirror. Had we used reflecting optics, there would be nothing available COTS, therefore it would have to be custom manufactured increasing cost significantly. A reflector would also complicate the relay optics significantly since we would not be able to use the pyramidal mirror.

In contrast, the refracting telescope has many advantages. It allows for a very simple relay optics. It is available COTS with high quality optics and is therefore relatively cheap. The FSQ-106N from Takahashi has been purchased. This telescope has significantly less chromatic aberration than other COTS telescopes. This is due to its four element design, two of which are fluorite. It has a diameter of 106 mm, and a 530 mm focal length, resulting in a total system focal length of 5300 mm.

2.5.3 Final Optical Layout

The current optical layout of the system is as follows. Light shines in through the sub-aperture. The light continues through the telescope until it hits the collimator which is inside the telescopes baffle. The light then goes through the collimating lens producing a 21mm diameter beam. The light exits and hits a reflecting mirror mounted onto a three axis FSM that acts as an ODL as well. The light is then reflected to the pyramidal mirror that is stationary. The light beam then enters the beam combiner, and is focused onto the CCD.

The FSM has to be able to compensate for any errors in its mounting. Therefore a high precision mount with a range up to 7 degrees was selected for the FSM actuators (See Table 2). The pyramidal mount is composed of two stages. The first stage provides all of the angular adjustments and the second handles X & Y translation in the entrance pupil of the beam combiner. The X-Y translation stage is small enough to fit behind the tip/tilt rotation stage and has the load capacity to hold both the second stage and the mirror. Any additional Z directional error can be offset by the FSM mounts.

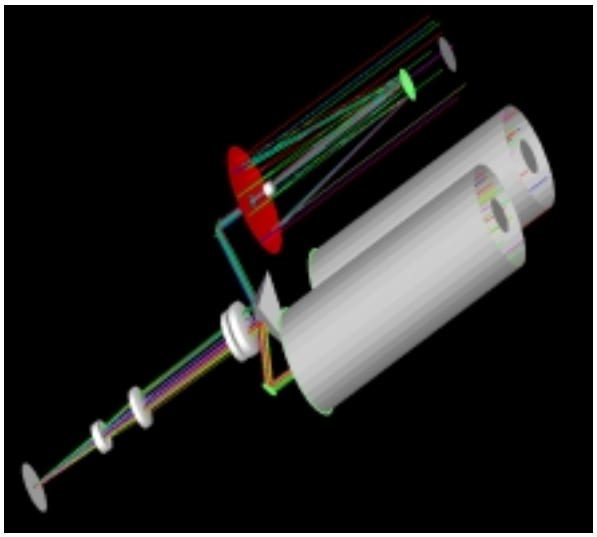

FIG. 13: 3D nonsequential ray-tracing using ZEMAX

TABLE 2: Actuator and mount specifications

Model	Angular Range	Angular Resolution	Linear Range	Linear Resolution
FSM	± 600 µrad	± 0.05 µrad	12 µm	0.2 nm
FSM Mount	± 7 °	± 0.0008 ° (± 14 µrad)	1 cm	1 µm
Pyramid Mirror Mount	± 4 °	± 2 arcsec (± 9.6 µrad)	13 mm	3 µm

2.5.4 Structural Misalignment Tolerancing

Using the mode of non-sequential ray tracing of ZEMAX, a complete ARGOS optics layout is constructed based on the optical specifications of a subaperture, pyramidal mirror, and the beam combining telescope as shown in Figure 13. We intentionally perturb the sub-telescope or pyramidal mirror to determine allowable structural misalignment, and we compensate the tilt error by changing the tilt angle of the fold mirror attached to the FSM. At 0.01 degree tilt of a subaperture, a pure FSM motion cannot restore the SR (Strehl Ratio) above 0.8. But the addition of FSM piston motion can restore the SR value to 0.859. We could achieve a SR of 0.859 (which is above diffraction limited) over 0.01 degree tilt. But due to a magnification factor 10, the

FSM compensation exceeded its max range (0.6 mrad=0.034 degree). Since we mounted a FSM onto a precision tip-tip mount which is capable of several arc-second adjustment (Table 2), this static error does not limit the FSM performance. However, it is much safe to have a FSM within a range of eliminating a possible maximum alignment error. 0.005 degrees or 15 arcsec for sub-telescope structural misalignment is suggested.

By assuming that all other optical components are perfectly aligned and the FSM can compensate all the residual tilt errors, the tilt errors for each surface of the pyramidal mirror are calculated. When the tilt error of the pyramidal mirror unit equals the tilt compensation of a FSM, the aberration loss due to the tilt is completely eliminated. Therefore there is no theoretical tilt tolerance for pyramidal mirror as long as it does not exceeds the maximum compensation range (0.01 degrees).

The beam combiner were tilted along x and y axis while leaving other optical components perfectly aligned (Figure 14). This beam combiner misalignment is not correctable by optical actuators like FSMs. However, it turns out that we can tolerate up to 0.2 degrees for the beam combiner, which is less stringent than other misalignment tolerances.

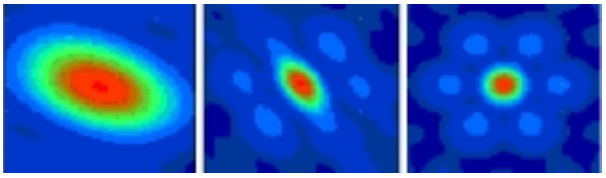

FIG. 14: The PSF plots when the beam combiner has tilt errors. From left to right, (1) X tilt: 0.2, Y tilt: 0.4 , (2) X: 0.3 Y: 0.3, (3) X: 0.25 Y: 0.25 [degrees]

3 Attitude Control System (ACS)

3.1 ACS Overview

The final ARGOS structure and the major ACS components are depicted in Figure 15. The Field of View of the CCD is 3 arc-minutes and thus to give us 1/2 arc-minute of margin on either side, the ACS subsystem is required to provide a pointing accuracy of +/- 1 arc-minute. The period of operation of the ARGOS system without human intervention must be 60 minutes or greater, meaning that the ACS system will have to either not saturate its actuators, or have some way of desaturating them within this given time span. The system must be able to slew at a rate of at least 1.5 degrees per second, placing a minimum requirement on the capabilities of the actuators to slew the spacecraft. Due to the nature of

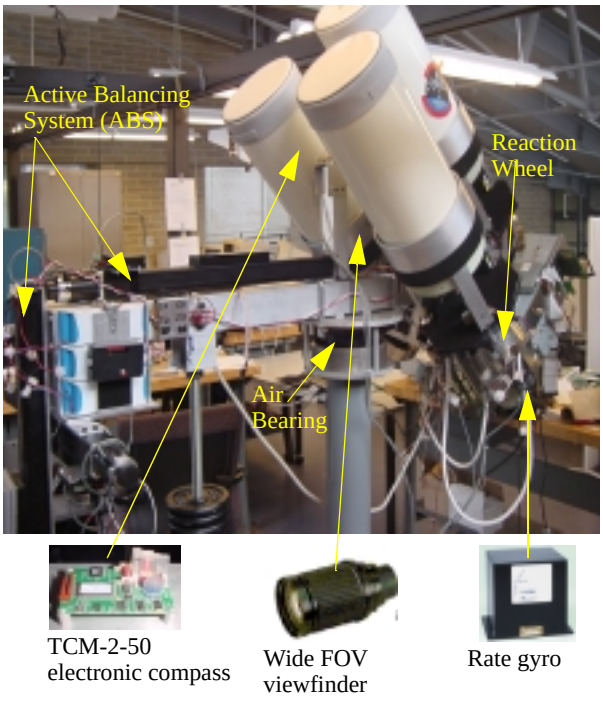

FIG. 15: The final ARGOS system with the three ACS sensors shown in the bottom

the ARGOS system, there will be some offset between center of gravity and the center of rotation, thus the system will need to have sufficient capabilities to overcome this torque.

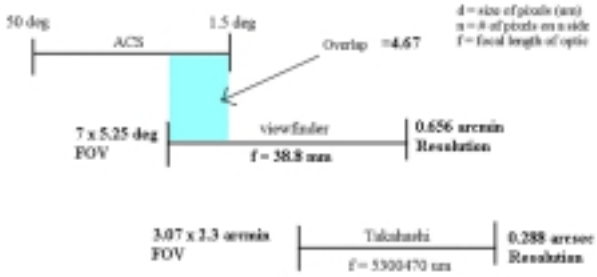

FIG. 16: Multi-staged ACS sensors

The sensor suite is composed of three integral elements. First, the TCM-2-50 electronic compass, with a 3-axis magnetometer, a 2-axis tilt sensor, and facilities to provide temperature information. Inclinometers/Electronic compasses measure the relative angles between the inertial coordinate frame and the body fixed frame. That is, they are used to give relative elevation, roll, and azimuth information between these two coordinate systems. The Inclinometer/Electronic compass is an

essential component of the coarse pointing sensor suite. Second, there is an intermediary sensor, which takes the form of a scope. It is a CCD that provides sufficient overlap with the ACS (Figure 16). Thirdly, there is a 3-axis rate gyroscope to run the reaction wheels.

3.2 Active Balancing System (ABS)

Due to the nature of the air bearing system chosen to simulate the space-based operation of ARGOS, the center of gravity and the center of rotation of the body will not necessarily be at the same position. The offset between their positions will impart a gravitational torque on the spacecraft, which will need to be overcome by the reaction wheels, both increasing their torque requirements as well as significantly increasing the angular momentum storage required by the reaction wheels, as this torque will be integrated over the period of operation of ARGOS.

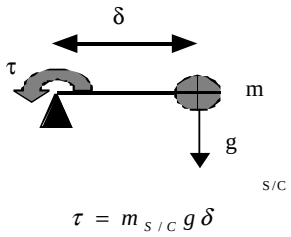

FIG. 17: Schematic of center of rotation, center of gravity offset, and gravitational torque.

The torque causes the wheels to increase in speed according to the equation:

$$\Delta\dot{\theta}_{wheel} = \frac{m_{s/c}\, g\, T_{desat}}{I_{wheel}}\,\delta$$

$\Delta\dot{\theta}$,the change in wheel speed before desaturation is required, is set by a combination of the limitations on the reaction wheel motor and the degree to which the wheels are balanced and T_{desat} is the time between desaturations and is set as a requirement for the overall ARGOS system. In designing the reaction wheels, it was intended to have the primary drivers be similar to those encountered in a space environment, and as such I_{wheel} should not be made much larger than would otherwise be required to control the dynamics of the spacecraft without having to overcome gravitational torques greatly exceeding those encountered in a space environment. In order to meet these constraints, the offset between the center of gravity and the center of rotation (δ) must be kept to on the order of 1 μm.

Statically balancing by designing for zero offset and using small ballast weights to make corrections may not be sufficient to achieve this. As such, an active balancing system, which can cause the overall spacecraft center of mass to shift, has been devised. The system can also be used to remove momentum from the wheels by intentionally causing an offset in the appropriate direction. This does not work about the vertical axis since one cannot put a gravitational torque about it, but there are also less disturbance torques about this axis, meaning that momentum build-up about this axis will be minimal. The selected active balancing system design is to use three linear motion slides based upon the custom developed lead screw and fixed servo system selected from the trades analysis. The slides are positioned on the end of the swing arm away from the telescope, as these do not represent a system that would be included on an actual satellite, and thus can be used to balance the center of gravity initially. Each of the slides will be mounted perpendicular to the other two, such that there are three independent axes of control of the position of the center of gravity (See Figure 15).

3.3 ACS Control System Design

A summary of the control design of the ACS subsystem is presented. Through the control method the attitude of the satellite can be deciphered and controlled. Initially the ARGOS satellite is at some arbitrary position, then the Science Operations and Communications subsystem provides reference information as to the position and behavior of the satellite by providing the ACS subsystem with the International Space Station's azimuth, elevation, range, azimuth rate and elevation rate. The ACS subsystem then converts this information into the body frame of ARGOS and then converts the input information into quaternion form. At the same time, two of the sensors being used, the rate gyroscope and electronic compass, are providing information as to the actual attitude of the satellite, this information is similarly ran through a function that transforms it into the body frame if necessary and then converts it to quaternion form. With this information the error in ARGOS's actual attitude can be computed and based on the desired and actual attitude information, how much the ARGOS system would need to rotate from its current body frame to the desired body frame would be known. The error quaternion is passed through an attitude controller which exhibits proportional, integral and derivative control; it is based on a non-linear control design. The output from the attitude controller is wheel speed and this is fed through an actuator system that outputs torque. This torque is then fed through the Attitude Control plant (the physical system) after which the body rate

and body rotation of ARGOS would be known. This information is then fed into the system's sensors.

Once the ISS is within the ACS viewfinder's field-of-view, the ACS system moves into the second mode. The centroding algorithm relays through the viewfinder the position of the ISS in (x,y) Cartesian coordinates. This viewfinder input is again transformed into ARGOS's body frame and converted into quaternion form. Thus in the second mode we only have rate gyro and viewfinder input. In both modes, a Kalman filter is used to provide the best representation of the actual system attitude by combining the input from the different sensors in the most optimal way, because for example, inclinometer input is best at low frequencies while rate gyro input is best at high frequencies, thus a mixing filter such as the Kalman filter becomes necessary to output the best combination of the two inputs.

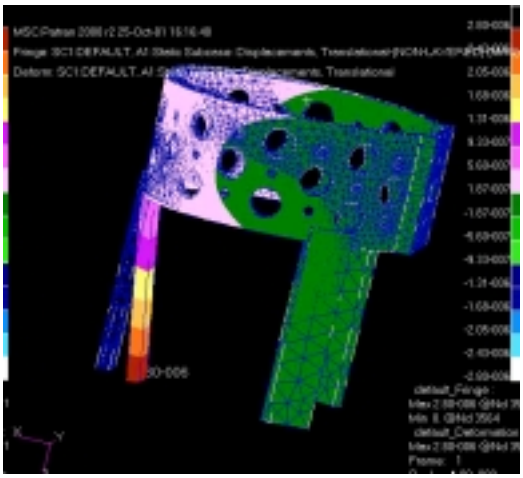

FIG. 18: Finite Element Analysis on Aperture collar

4 Structures

4.1 Aperture Alignment System

From the discussion in the section 2.5.4, a subaperture mount needs to provide an alignment accuracy of 15 arcsec. Based on the collar design, there are 3 mounting points for the actuators. One mounting point is located at the base of each leg. An assumption was made that the aperture collars could be manufactured to provide an alignment tolerance of 1 degree. Based on this maximum of 1 degree offset, the actuators will need to have a minimum range of 3.39 mm and will need to accommodate for a 30 micron deflection. The actuators will also need to have a resolution of 15 microns based on the 15 arcsec alignment requirement.

Figure 18 shows deflections seen from a 500 N load applied radially inward at the bottom of one of the legs. The deflections are not drawn to scale. The Color coding on the right side of the screen represents the actual deflections seen by the collar. According to this FEM analysis, the 500 N load would cause a 3 micron deflection rather than 30 microns as expected. This told us that our simple cantilever beam model was too simple and that the stages would have to withstand higher loads for the required deflections. We decided to build the Collar and aperture alignment system to test if the translation stages could withstand these higher loads.

To test the alignment capabilities of the translation stage system, a laser pen was attached to one of the telescope assemblies. The laser was aimed at a target with calibrated lines on it. The translation stages were adjusted to their limits and the distance traveled by the laser point was measured. The distance from the center of rotation of the telescope to the target was also measured. Using these two values, the alignment capabilities of the translation stage system was calculated to be 3 degrees.

The translation stage aperture alignment system meets all of the requirements. Each stage has a resolution of 10 mm, which beats the 15-mm requirement. The system also allows for a maximum alignment of 3 degrees, which beats the 1-degree requirement. Additional springs were added to the translation stages to prevent the apertures from tipping during operations.

4.2 Other Structural Requirements

4.2.1 Modularity

A major requirement of this project is modularity. Modularity has been defined to include three main things. The first is the use of replicated components that simplify the design and manufacturing process. These replicated components should be able to serve a greater function when connected. Secondly, a modular system should have quick connections. These connections should be simple, easily accessible, and detachable. Finally, the modules should have high-density packing. The satellite should be able to separate into modules that allow for compact packing. This will allow for the most efficient use of space in a launch vehicle or in transport to a testing location.

4.2.2 Segregation of optics from bus subsystems

A requirement was set that the bus subsystems be isolated from the optics. Issues such as vibrational disturbances, heat contamination, and electromagnetic interference raised concerns for the optics team. Therefore, the requirement was set that the bus subsystems be placed as far away from the optics as possible.

4.2.3 Derived Requirements

First, it is determined that the central combiner telescope must be located below the central plane of the satellite. This requirement leads to the need for a swing arm so that the air-bearing pedestal does not interfere with the satellite. Second, the optics has placed a requirement that the sub-apertures be aligned within 15 arc seconds. This requirement created the need for a manual aperture alignment system.

The general structure consists of 3 aperture modules and 1 combiner module. The 3 aperture modules attach to the central combiner module to form the satellite. The satellite's center section can then be attached to the swing arm to simulate space conditions. Since this is a ground system, it was determined that certain non-flight components such as batteries and the static and active balancing systems could be placed on the opposite side of the swing arm. These items will provide a counterbalance to equalize the weight on the swing arm, while still maintaining a valid simulation of a space system.

4.3 Final Design

4.3.1 Aperture Modules

ARGOS contains three Aperture Modules. Each Aperture Module contains a telescope, Fast Steering Mirror (FSM), Reaction Wheel, Reaction Wheel Motor, and Reaction Wheel Controller. All Aperture Modules are exactly the same except for a miscellaneous section symbolized by the box on the bottom of the CAD drawings below. The miscellaneous section of Aperture 1 (A1) contains the Computer. The miscellaneous section of A2 contains the FSM Amplifiers. The miscellaneous section of A3 contains the Rate Gyro.

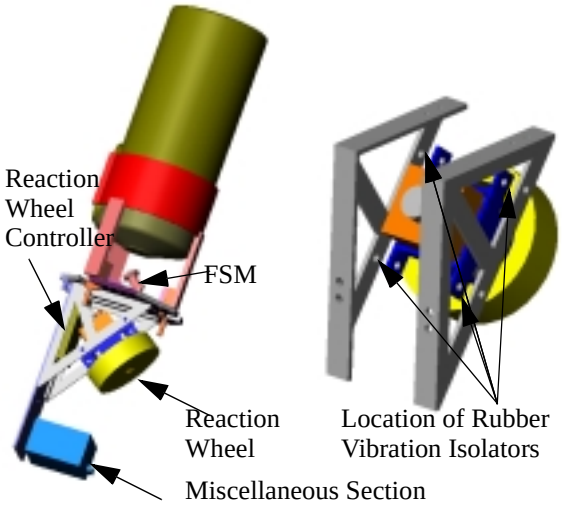

FIG. 19: Aperture module (left) and RWA module (right)

4.3.2 Reaction Wheel Module

The main challenge in designing the reaction wheel mounts was determining an adequate method of suppressing the vibrations caused by slight imbalances in the wheels. Since a solid metal attachment would translate most of the vibrations, a variety of rubber vibration control mounts were examined. The mounts we chose have a tapped hole to accept a screw on one end of the rubber and a screw of the same size protruding on the other end.

4.3.3 Center Combiner Module

The third module of ARGOS is known as the Center Combiner Module (CCM). The CCM holds the Combiner Telescope, the Pyramidal Mirror, the View Finder and the CCD. A series of tip/tilt stages provides rotational control in all axes of freedom and translational control parallel to the central axis. Three clamps that are tightened with ball-bearing tipped setscrews hold the Combiner Telescope. The ball bearings allow the set screws to push the clamps radially inward towards the telescope without rotating the clamps.

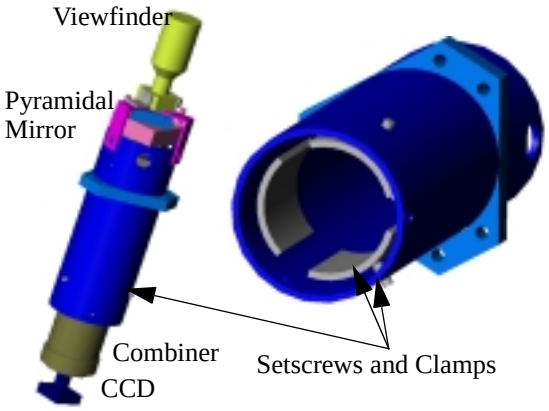

FIG. 20: Center Combiner Module (CCM)

4.3.4 Module Interfacing

ARGOS is assembled by attaching the three Aperture Modules to the Center Combiner Module. Each Aperture Module has two locating pins and a through hole for a screw. The Center Combiner Module contains two holes for the pins to drop in for each aperture as well as a tapped hole at the bottom so that the modules may be tightened into place.

4.3.5 Swing Arm

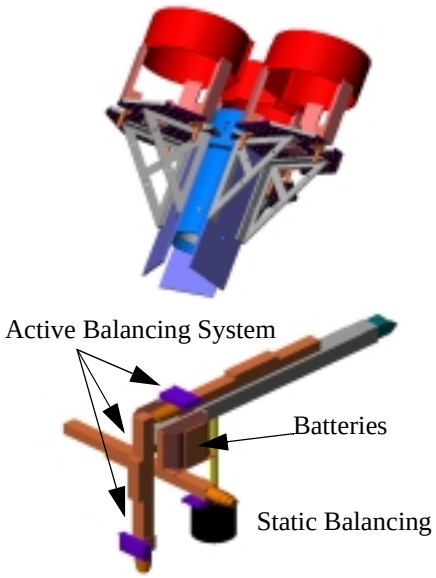

FIG. 21: Assembled aperture mode and swing arm design

In order to build a ground version of this satellite and have it float on an air bearing, a swing arm had to be used. The presence of gravity also created the need for things such as the static and active balancing systems to control the location of the center of mass of the spacecraft. Since these systems would not be found on the flight version of ARGOS, they were placed on the opposite side of the swing arm to counterbalance it on the air bearing. The batteries were also placed on the far side of the swing arm since a different power system including solar panels would be used in the flight version of the spacecraft.

5 Avionics

Figure 22 contains the ARGOS avionics hardware schematic. The optics systems we have to interface with are in yellow, the ACS systems are in blue, and the Science/Operation/Communications systems are in purple. The number of COTS components that require standard PC interfaces has driven our decision to make use of a standard PC motherboard as the base of our avionics system. Sensor readings will be put into the PC's memory to be accessed by the HERON4 DSP when necessary for control purposes.

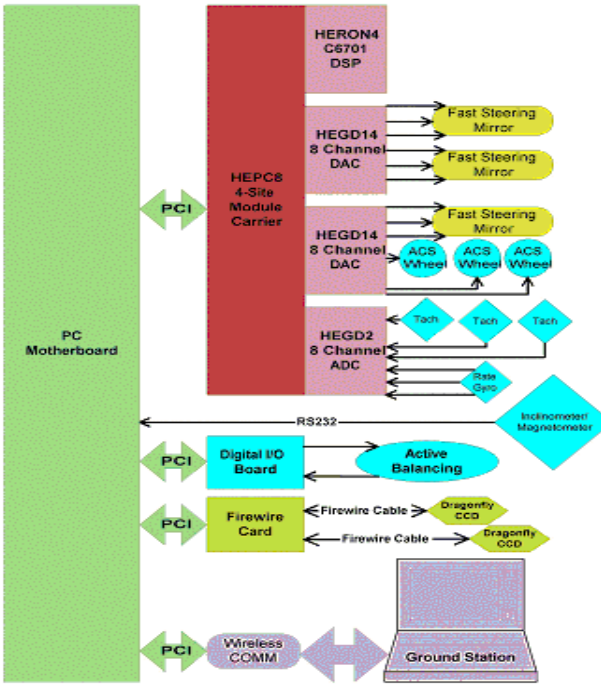

FIG. 22: Avionics hardware schematic

The HEPC8 houses our HERON4 digital signal processor (DSP) in its first slot. The other three slots are free for expansion modules. To meet our I/O requirements, we are using two HEGD14 8-channel DACs and one HEGD2 8-Channel ADC. The satellite's actuators are connected to the DAC modules, because they must be driven by analog signals. Each fast steering mirror will

sit on a set of three piezoelectric actuators that require a signal a voltage signal per actuator. Each ACS wheel will require one signal to control its spin, which in turn will spin the entire satellite. Most of the satellite's ACS sensors are connected to the ADC modules, because they provide analog signals that must be understood by the computer as digital signals. Three tachometers will provide data on how fast each ACS reaction wheel is spinning. A three-axis rate gyro assembly will provide data on how fast the entire satellite as a whole is spinning. The computer will use this data when deciding what signals to send to the reaction wheels to affect the satellite's movement. The remaining ACS sensor is the inclinometer/magnetometer that gives us a data on the satellite's pitch and compass heading. While it does have a choice of analog or digital outputs, it does not fit on our ADC card. Instead, we are connecting it directly to the PC motherboard using a standard RS232 serial port. This may create a problem in the future if these readings cannot be passed from the PC to the DSP fast enough to control the system smoothly, but since it is the only critical ACS sensor on board the PC, we may be able to predict its readings from the tachometers and rate gyros on board the DSP if this loop frequency needs to be higher than we can manage to deliver. Three other COTS components connect directly to the PC motherboard as well. The active balancing system (ABS) is self-contained within a single specialized I/O board that connects to the motherboard via a standard PCI slot. It will take data from the computer based on other sensors, and send voltages to the ABS actuators to move balancing weights. The main CCD camera and the viewfinder CCD camera will both connect to the same PCI interface card. Finally, the wireless LAN card we are using for remote operation also interfaces with the PCI slot.

To meet the requirement of simultaneous automatic control of various subsystems, ARGOS will be tracking the International Space Station (ISS) as it crosses the night sky. In order to do the image processing necessary to track moving objects with the satellite, we needed to get the most powerful PC we could find. We also needed to load it with as much RAM as we could afford to avoid slow hard drive data writes. Our goal in designing the PC system was to make one that would not need to access a slow, heavy, power hungry hard drive. The combination of an AMD 1.4 GHz Athlon processor on a Shuttle AK31 motherboard will go a long way towards fulfilling this requirement. The AK31 can operate at a front side bus (FSB) frequency of 266 MHz, which helps to alleviate the biggest bottleneck in PC performance - the time between when data is requested from memory and when it is delivered. Also, the AK31 features a highly configurable jumperless BIOS that gives us the opportunity to easily overclock the CPU, FSB, or memory if processes are taking too long.

6 Conclusion

The ARGOS is successfully designed and integrated into the full structure ready to operate. The optics controller utilizing model-based control and neural network is under development. A preliminary assessment shows that the beam combining problem is the most challenging aspect of sparse optical arrays. The need for optical control is paramount due to tight beam combining error tolerances. The wavefront sensing/control requirements appear to be a major technology and cost driver. The ARGOS testbed uniquely addresses the real world problems such as the vibrational coupling between a spacecraft structure and the wavefront errors propagating through the whole system. If ARGOS succeeds in coherent beam combining, it will be the first sparse aperture array obtaining a phased image of a real imaging target in the sky.

References

[1] Meinel, "Cost Scaling Laws Applicable to Very Large Telescopes", SPIE, 1979.

[2] Golay, M., "Point Arrays Having Compact Non-redundant Autocorrelations", J.Opt Soc. Am., vol. 61, pp 272, 1971.

[3] Powers, M. et al, "Assessment of a Large Aperture Telescope Trade Space and Active Optomechanical Control Architecture", Proceedings of the 1997 IEEE Aerospace Conference, pp 197-229, Feb 1-2, 1997.

[4] Harvey, J.E., Silverglate, P.R., and Wissinger, A.B., "Optical Performance of Synthetic Aperture Telescope Configurations", Southwest Conference in Optics, pp 110-118, SPIE vol. 540, 1985.

[5] Chung, S.-J., "Design, Implementation and Control of a Sparse Aperture Imaging Satellite", Master of Science Thesis, MIT, 2002.

[6] Faucherre, M., Merkle, F., and Vakili, F., "Beam Combination in Aperture Synthesis from Space: Field of View Limitations and (u,v) Plane Coverage Optimization", New Technologies for Astronomy, pp 138-145, SPIE vol. 1130, 1989.

[7] De Hainaut, C.R. et al, "Wide Field Performance of a Phased Array Telescope", Optical Engineering, vol. 34 No.3, March 1995.

[8] Zarifis, V., et al, " The Multi Aperture Imaging Array", ASP Conf. Series 194, Working on the Fringe: Optical and IR Interferometry from Ground and Space, Unwin

and Stachnik, eds, pp. 278.

[9] Hill, J.M., and Salinari, P., "The Large Binocular Telescope Project", Astronomical Telescopes and Instrumentation, pp 36-46, Munich, Germany, March 2000.

[10] Roddier, F., and Ridgway, S., "Filling Factor and Signal-to-Noise Ratios in Optical Interferometric Arrays", The Astronomical Society of the Pacific, III, pp 990-996, August 1999.

[11] Fienup, J.R., "MTF and Integration Time versus Fill Factor for Sparse-Aperture Imaging Systems", Proceedings in Imaging Technology and Telescopes, Proc.SPIE 4091A-06, July 2000, Sandiego, CA.

[12] Harvey, J.E., and Rockwell, R.A., "Performance Characteristics of Phased Array and Thinned Aperture Optical Telescopes", Optical Engineering, Vol. 27 No.9, September 1988.

[13] Mennesson, B., and Mariotti, J.M., " Array Configurations for a Space Infrared Nulling Interferometer Dedicated to the Search for Earthlike Extrasolar Planets", ICARUS 128, pp 202-212, 1997.

[14] Smith, W.J., "Modern Optical Engineering", 3rd ed, McGraw-Hill, 2000.